Unprecedented Insight into the Thermal Processing of a Blast Furnace

B. Peters[a)], X. Besseron, P. Adhav

Department of Science, Technology and Medicine, University of Luxembourg.

[a)] Corresponding author: bernhard.peters@uni.lu

Abstract. Although the steel industry undergoes a transition from traditional blast furnace technology to "green" steel, the blast furnace and its variants produce still the largest amount of steel. Hence, a thorough understanding of the internal process of a blast furnace is indispensable for improved performance, in particular, facing challenges of hydrogen injection. The current simulation platform derived from the extended discrete element method (XDEM) with its detailed resolution of the blast furnace processes based on first principles closes a mayor knowledge gap and, thus, allows for a digital twin of blast furnaces. An Euler-Lagrange coupling forms the platform for the simulation framework, in which coke and iron-bearing material is treated dynamically and thermodynamically as individual entities in the Lagrangian frame of reference, whereas the multi-phase flow regime in the interstitial space is described through Computational Fluid Dynamics (CFD). Both, multi-phase flow and particulate material interact by heat, mass and momentum transfer. A thorough analysis of the high resolution results unveils the internal physics of a blast furnace and, thus, becomes an integral tool for design and operation within a smart virtual prototyping (SVP) environment of the digital twin technology (DTT).

INTRODUCTION

State-of-the-Art

There are essentially two types of numerical methods for modelling multi-phase flow phenomena involving a solid, such as a particulate phase: On a macroscopic level, all phases are treated as a continuum, with the two-fluid model being its most well-known representative [24]. The second approach relies on an Euler-Lagrange coupling in which the particulate phase is treated as discrete entities and the void space around the particles is described usually by computational fluid dynamics.

Because of its easy computation and effectiveness of the former, it is a good fit for process modelling. However, the averaging concept greatly reduces the amount of information available about the size distribution, shape, or material characteristics of individual particles. Therefore, this loss of information on particles i.e. small scales has to be compensated by additional constitutive or closure relations.

However, current computer resources and recent advances in research by [32, 37, 41, 64, 67, 69] allow now an Euler-Lagrange approach describing the particulate phase by a discrete method and thus, provide a deeper insight into the underlying physics. After reviewing mathematical modeling of the raceway, shaft processes, hearth, and top charging, Shibo et al. [33] concluded that research still focuses on individual blast furnace processes rather than highlighting an integral modeling platform for the complete blast furnace. In order to optimize operating conditions, Zhou et al. [92] characterized the shaft, raceway, and hearth using separate CFD models. A three-dimensional CFD model was used by Lulu et al. [30] to somewhat offset the previously noted fragmented modeling methodologies. Both in industrial and experimental settings, it could forecast furnace states, and the predictions generally agreed with measurements. Dong et al. [22] used a CFD model in conjunction with the ore's temperature distribution to determine the cohesive zone's location. Shen et al. [80] investigated reduction degree and gas utilisation as key performance parameters with a CFD model.

Similarly, the author initially analysed and validated single processes of the blast furnace e.g. reduction in the shaft area [19, 56, 61, 62, 63], multiphase flow in the dripping zone [8, 9, 10, 11], softening and melting in the cohesive zone [12] and raceway formation and behaviour [4, 76]. From its very inception, the cutting-edge XDEM simulation platform was created to describe physical phenomena such as melting or chemical conversion rather than concentrating on particular applications. Thus, the same physical phenomena are independent of any engineering applications which enhances its versatility and re-usability as carried out in for example [49, 53, 55]. For a more detailed review, the reader is referred to Peters [54].

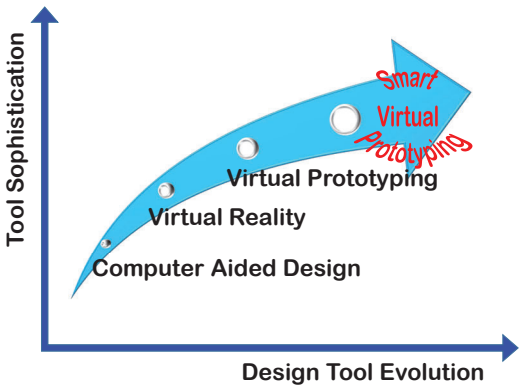

FIGURE 1. Advancing the evolution of design tools to the next higher level of sophistication through virtual prototyping with a digital twin.

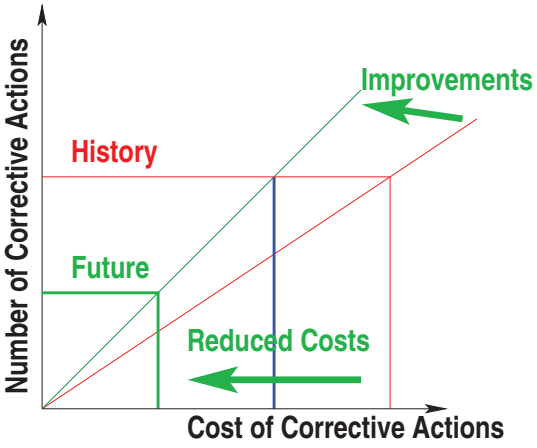

FIGURE 2. Improvements through a digital twin technology leads to significantly less corrective actions i.e. costs

Digital Twin Technology for Blast Furnaces

Modelling of and software for single-physics applications in conjunction with an ever increasing computational power have reached a level of maturity that allows combining them for multi-physics applications. This trend is in line with an almost natural evolution in design tools: starting from computer-aided design (CAD) and engineering (CAE) in the beginnings and boosting virtual reality (VR) and prototyping (VP) to the next level of sophistication of smart virtual prototyping (SVP) by a digital twin as depicted in Fig. 1. Consequently, this article addresses smart virtual prototyping in form of a digital for a blast furnace.

In addition to engineering requirements, societal needs demand digital twin technology i.e. smart virtual prototyping that allows a shift from current empirical-based practice to an advanced multi-physics simulation technology. Often, engineers opt for "copy & paste technology" of already proven components and systems from previous generations. It results in a conservative design with little potential for innovative ideas. These limitations are removed by virtual prototyping.

In addition, smart virtual prototyping has a strong impact on science, economics and society for which high-performance-based computer simulations are a fundamental drivers. The driving force for introducing digital twins in industry is to reduce significantly the time-to-market and costs. It gained a degree of importance to business that the digital twin is among "Gartner's Top 10 Strategic Technology Trends for 2017" [1]. Thus, improvements through digital twin technology reduce both number of corrective actions and consequently their costs as shown in Fig. 2.

Furthermore, digital twins remove the constraints of physical prototyping namely time, costs and conservative design. If at all, only a reduced number of physical prototypes is required with shorter testing phases. Similarly,

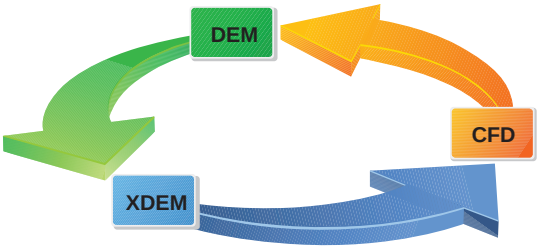

FIGURE 3. Integrated Simulation Platform consisting of the "best-of-the-class" modules coupled.

information from digital twins already available at an early stage of design avoids costly re-designs. Problems are identified before they even occur, down-times are reduced leading to a faster time-to-discovery and time-to-solution.

While already high performance single-physics software platforms for computational fluid dynamics (CFD) as mentioned by Phuc et al. [65] and discrete element method (DEM) including thermodynamics of the particulate phase, referred to as extended discrete element method (XDEM) and summarised by Peters [55] exist, an integrating framework for executing discrete and continuous single-physics modules in a highly scalable parallel mode does not exist. A deployment of a highly performing multi-physics framework is hindered by the fact that a simple coupling of two or more parallelised modules ends in a sequential application because data between individual modules is not exchanged. Rather than developing an "all-in-one" multi-physics software platform i.e. single code, a coupling of "best-of-the-class" single-physics software modules in a multi-physics coupling framework for engineering applications is preferred as depicted in Fig. 3.

Consequently, the XDEM software, representing the DEM and XDEM module as the discrete phase and OpenFOAM describing the fluid phase as a CFD module in fig. 3 are representative candidates for developing a generic multi-physics coupling framework. Such a concept can be easily extended by additional modules such as FEM and was carried out by Peters et al. [2]. This methodology paves the path towards smart virtual prototyping that comprises a particulate phase in contact with a fluid phase. It closes a technological gap and has the potential to revolutionise design and operation of plants and factories impacting heavily on society.

MATHEMATICAL FRAMEWORK

The addressed extended discrete element method (XDEM) is derived from the discrete element method (DEM) by extending it with the thermodynamic state of a particle. Hence, the simulation platform comprises three modules as shown in Fig. 3:

1. XDEM: The XDEM module evaluates the thermodynamic state of a particle with one-dimensional and transient differential conservation equations. For this purpose a simplified set consisting of transport equations for mass, energy and momentum is solved as described in detail by the author [51]. The solution of this system of conservation equations yields a distribution of temperature and species inside a particle that essentially governs additional conversion process such as homogeneous/heterogeneous reactions and phase change such as evaporation e.g. drying, melting or coating. Thus, the thermodynamics module has proven its versatility and reliability for numerous applications in thermal processing of particulate material.

2. DEM: The DEM-module essentially describes the downward motion of the ore and coke particles. Like traditional DEM technology, it offers a selection of impact, rolling and attraction models for different particle shapes e.g. cylinders, discs, cubes or ellipsoids accompanied with a given size-distribution as described by the Sameie and Peters [52, 75]

3. CFD: Although any CFD module may be applied and coupled to evaluate the flow in the interstitial space, OpenFoam's reacting multi-phase solver was selected. It allows to describe the multi-component gas phase

with its reactions and the two phases for liquid iron and slag taking into account the phase interactions. For more details, the reader is referred to the homepage of OpenFoam.

Each of these three modules fulfills a particular task in the multi-physics simulation for a blast furnace: The XDEM module evaluates the thermodynamic state of each particle in the blast furnace, while the DEM module describes the slowly descending burdens i.e. coke and ore layers in the furnace. The void space between the particles is represented by a multi-phase flow of gas and two liquids namely liquid iron and slag. Thus, the physics are described accurately by the best modelling approaches for each domain. The three modules are coupled to exchange mass, heat and momentum between the particulate and fluid phases. Both, DEM and XDEM module are parallelised through a hybrid approach based on the message passing interface MPI and OpenMP [66]. This approach allows a significant fast throughput of simulation cases by exploiting the particular architecture of a computer with either several processors allowing a partitioning of the domain for applying MPI or/and using a desired number of threads per processor for OpenMP.

The distribution of relevant variables is described by transient, one- and three-dimensional conservation differential equations for both, the discrete and continuous phase which are summarised as follows:

Continuity Equation

$$\frac{\partial}{\partial t}(\alpha_i \rho_i) + \nabla \cdot (\alpha_i \rho_i \vec{v}_i) = \Sigma_{j=1}^{n} \dot{m}_{ij} \tag{1}$$

where ρ_i and $\vec{v}_i$ denote the density and velocity of phase i, respectively. The right hand side summarises the mass transfer between phases, in particular, the exchange of gaseous species and liquids between the particulate and continuous phase.

Momentum Equation

$$\frac{\partial}{\partial t}(\alpha_i \rho_i \vec{v}_i) + \nabla \cdot (\alpha_i \rho_i \vec{v}_i \vec{v}_i) = -\alpha_i \nabla p + \alpha_i \rho_i g + \nabla \cdot [\alpha_i \mu_i (\nabla \vec{v}_i + \nabla (\vec{v}_i)^T)] + \dot{m}_i \vec{v}_i - \vec{F} \tag{2}$$

where p, g, μ_i, m_j, $\vec{v}_j$ and $\vec{F}$ stand for pressure, gravity, viscosity, mass introduced with its velocity into the phase i and external force, respectively.

Energy Equation

$$\frac{\partial \alpha_i \rho_i h_i}{\partial t} + \nabla . (\alpha_i \rho_i \vec{v}_i h_i) = -\nabla \cdot (\alpha_i \kappa \nabla T_i) + \frac{\partial p}{\partial t} + \vec{v}_i \cdot \nabla p + \nabla \cdot (\vec{v}_i \cdot \vec{\tau}) + \dot{m}_i h_i + \dot{Q}$$

where κ, T_i, $\vec{\tau}$, $\dot{m}_j$, h_j, $\dot{Q}$ refer to heat conductivity, phase temperature, stress tensor, mass flux introduced in to phase i with its enthalpy h_j and a heat source e.g. a chemical reaction releasing or consuming energy.

Gas Species Transport Equation

The gas phase is considered as a multi-component mixture that undergoes chemical reaction whereas the liquid phases are treated as pure phases.

$$\alpha_g \frac{\partial Y_{g,i}}{\partial t} + \nabla \cdot (\alpha_g Y_{g,i} u_g) = \nabla \cdot \left(\alpha_g D_{g,i,eff} \nabla Y_{g,i}\right) + \dot{Y}_{g,i} \tag{3}$$

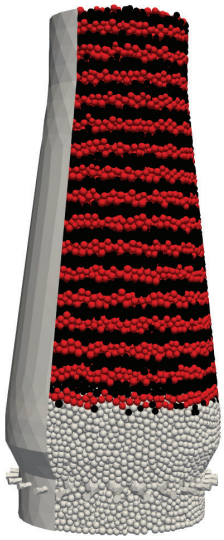

FIGURE 4. Production blast furnace with hearth coke (grey), iron ore (red) and shaft coke (black) layers (shaft and hearth coke are coloured differently for visualisation purposes only)

where $Y_{g,i}$, $D_{g,i,eff}$, $\dot{Y}_{g,i}$ are specie mass fraction, diffusion coefficient of specie i and a specie source due to chemical reactions, respectively. The liquids are currently pure phases so that a transport of species within the liquids is not required. These conservation equation are discretised by the finite volume method (FVM) [21, 46] leading to linear equation systems (LES) that are solved by appropriate solvers involving pre-conditioning.

The particle's position and velocity are obtained by the classical discrete element method (DEM) [16, 59] based on Newton's law. For a detailed description of the physics including numerical aspects, the reader is referred to Peters et al. [51, 59].

ANALYSIS OF A PRODUCTION BLAST FURNACE

The following sections describe set-up including initial and boundary conditions, predicted results on both a single ore particle and the entire blast furnace.

Setup of Simulation Case

The blast furnace has a height of 25 m and a belly diameter of 14 m. In order to handle a blast furnace, which usually contains a particle number of the order of 10^9, the coarse grained (CGM) and representative particle method (RPM), packing app. 1000 particles into a parcel, for motion and thermal conversion, respectively, were applied [54]. Hence, in a first step, the blast furnace was filled with coke and ore particles through a pure DEM simulation which resulted in an initial layered structure of ore and coke material in the upper part of the blast furnace and the hearth filled with coke as shown in Fig. 4.

In order to shorten the heating-up period of the blast furnace, both the gas and the particulate phase were initialsed with a linearly increasing temperature from top to bottom. The top temperature was set to 600 K while the bottom temperature was 2200 K.

Granular material in the blast furnace moves downward very slowly under the influence of gravity so that the mechanical properties of coke and ore are set identically. Both, normal and friction forces were considered by a

linear-spring-dashpot model [75] for which relevant material properties are given in table 1 and are derived from Watakabe et al. [85].

TABLE 1. Mechanical and thermodynamic properties of coke and ore particles

Property	Unit	Coke	Iron Ore
Number of particles	[-]	36989	13556
Particle diameter	[m]	0.138 - 0.2	0.138 - 0.2
Particle density	[kg/m³]	150	2401.6
Thermal conductivity	[W/mK]	0.165	17.05
Specific heat	[J/kgK]	355.16	331.3
Poisson ratio	[kg/ms]	0.45	0.45
Restitution coefficient	[-]	0.1	0.1
Friction coefficient	[-]	0.1	0.1
Young's modulus	[N/m]	$5{\cdot}10^8$	$5{\cdot}10^8$

Reduction of iron oxides with carbon monoxide and hydrogen follows the reaction equations 4 to 6

$$3Fe_2O_3 + 2\,CO/H_2 \leftrightarrow 2Fe_3O_4 + 2\,CO_2/2\,H_2O \tag{4}$$

$$Fe_3O_4 + CO/H_2 \leftrightarrow 3FeO + CO_2/H_2O \tag{5}$$

$$FeO + CO/H_2 \leftrightarrow Fe + CO_2/H_2O \tag{6}$$

for which the details of the reaction mechanism in particular kinetic data is summarised in [27]. The integral reaction rate is composed of a backward and forward rate depending on local inner-particle gas composition and temperature so that the reduction degree follows the Baur-Glässner diagram. In addition, the Boudouard reaction

$$C + CO_2 \leftrightarrow 2\,CO \tag{7}$$

is taken into account, which recycles formed carbon-dioxide from the reduction of iron oxides to carbon-monoxide in the coke layers for further reduction.

The above-mentioned reaction mechanism was validated over a temperature range between 1072 K and 1272 K for five different compositions of the reducing gas and is shown for a representative temperature of 1173 K in the following Fig. 5. Iron oxides were reduced under pure carbon monoxide and hydrogen and three mixtures of both reducing agents. Fig. 5 shows a very good agreement between predictions and experimental data represented by symbols considering that only one reaction mechanism with identical kinetic data over the entire temperature and composition range was applied. The results in the following sections were obtained under a reducing atmosphere with carbon monoxide only. This reaction mechanism is applied for each iron ore particle in the blast furnace so that the reduction progress for each particle is governed by local heat and mass transfer conditions from the hot blast.

The CFD mesh consists of 116640 cells and the tuyeres blast flow was evaluated as 4.8 Nm^3/s that was introduced at a temperature of 2540 K and composed of 21% oxygen and 79% nitrogen. Although the XDEM simulation platform has the capability to predict raceway phenomena, it was excluded from the current study to keep the computational time in bounds with the resources available. However, detailed investigations for the formation of a raceway have been carried out by the author [4, 77] so that the shape of the raceway was pre-set as sphere-like in a first step. Similarly, the thermodynamics of a raceway were not resolved and, therefore, the heat release of the PCI combustion was converted to a representative inlet temperature. A validation of all individual processes occurring in a blast furnace and a complete validation with data from an experimental blast furnace [86] were carried out and are described by Peters [54].

Results and Discussion

Thermodynamic State of an Individual Ore-Particle in a Blast Furnace

The following Fig. 6 depicts the temperature profile over a chosen period of 900 s i.e. 15 mins. Although the lifetime is much longer, the period of 15 mins is sufficient to highlight the key features. The particle temperature was initialised

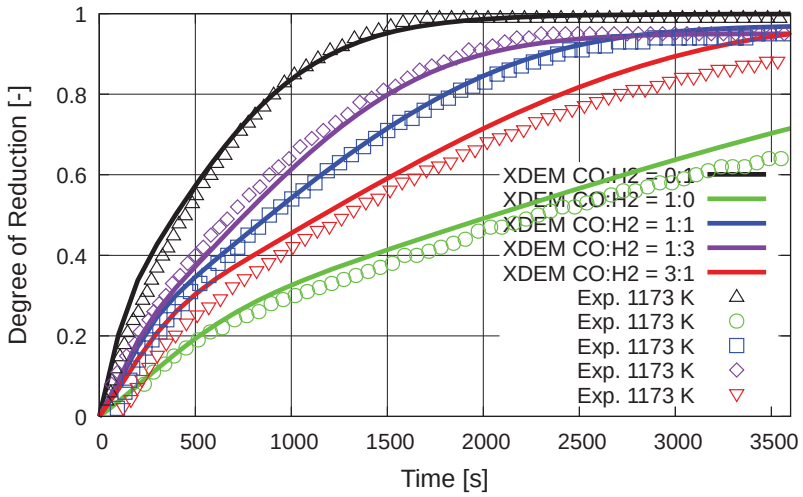

FIGURE 5. Reduction degree versus time for a single particle at a temperature of 1173 K for differently composed reduction gases

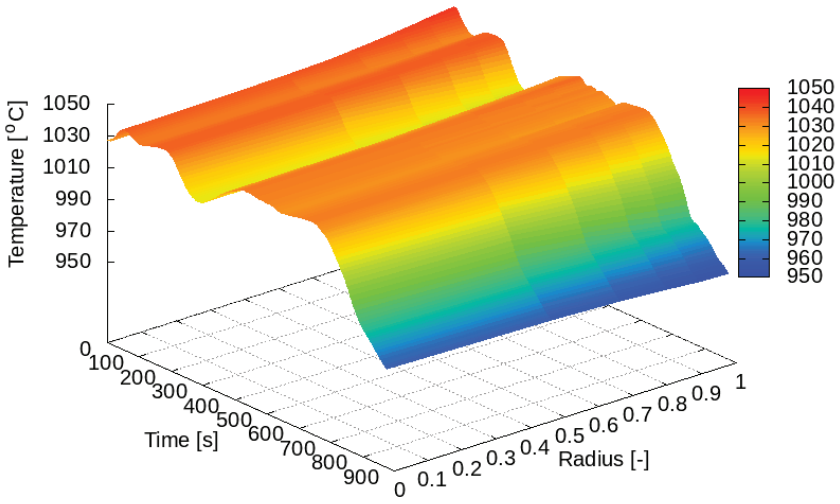

FIGURE 6. Temperature profile versus time and radius in an ore particle near the cohesive zone

to app. 950 ^{o}C after which the particle surface and interior temperature is governed by the heat transfer from the gas and the endothermic reducing reactions. The latter explain the local temperature minimum at app. 300 s. Although the particle temperature experiences minor interior gradients, the entire temperature has a strong transient behaviour.

This is similarly reflected by the reaction rate i.e. formation rate of magnetite shown in Fig. 7. In addition to temperature fluctuation and consequently to heat transfer conditions as shown in Fig. 6, the reduction rate is also effected by the mass transfer of carbon monoxide as a reactant and carbon dioxide as a product of the reduction process. Hence, the formation rate undergoes also a very transient behaviour determined by the varying gas temperature and composition in the vicinity of the particle in question. The transient behaviour of the reaction rate extends into the particle by app. 20 % of the particle radius. Obviously, it resembles neither a shrinking core with reactions only taken place at the particle surface nor a reacting core behaviour with reactions occurring inside the entire particle, and therefore, cannot

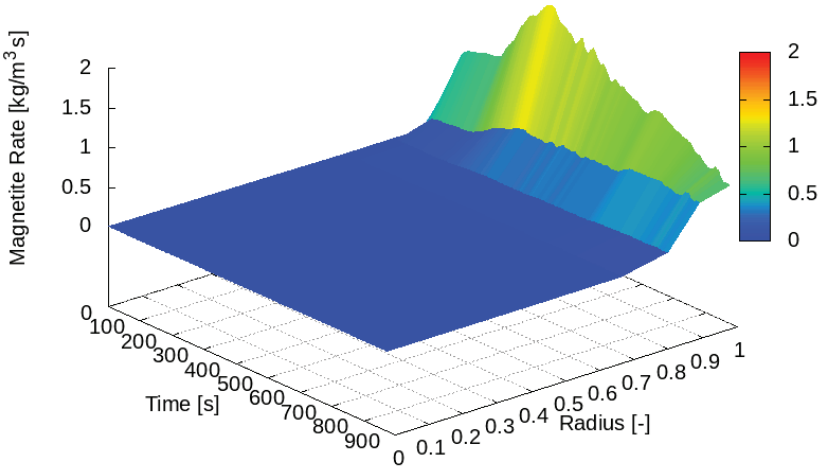

FIGURE 7. Reaction rate profile of magnetite versus time and radius in an ore particle near the cohesive zone

be assumed in advance as a reaction mode. A pre-defined reaction mode results in erroneous reaction rates eventually leading to an incorrect production rate.

The current approach of resolving internal particle properties such as temperature or species distributions with a uniform or, as in the current case chosen, with a non-uniform mesh with more cells clustered at the boundary, stresses the necessity for inner particle discretisation. Only with this feature available, the particles are enabled to adjust to the prevailing boundary conditions, expressed through the Biot and Peclet numbers for heat and mass transfer, respectively, and adapt to the physically correct representation of the reaction state varying between the two extremes of reacting and shrinking core mode.

Finally, Fig. 8 depicts the evolution of magnetite stemming from the reduction of haematite. Since, the magnetite mass is the cumulated mass versus time of the reaction process, fluctuations are less visible in the magnetite profile of Fig. 8 and it basically has a steadily increasing characteristic.

Analysis of a Blast Furnace

Under the above-mentioned conditions with an assumed linear temperature profile over the height of the blast furnace taken from previous simulation results, the entire blast furnace model was run for a real time period of 20 min, which indicated quasi-steady state conditions for the production rate as depicted in Fig. 9. These 20 min of real time required a computer runtime of 44 cpu-hours with 8 partitions on one *AMD* $Epyc^{TM}$ $7H12$ node providing 128 cores and clock speed of 2.6 GHz, which is a more than acceptable computational time considering the sheer size of the reactor. After these first experiences, potentials for speed-up have been identified that promise a further reduction by a factor of app. 2-3. It allows running the blast furnace for hours in real time and investigating deeper into operating conditions. Fig. 9 shows clearly the evolution of the production rate as an integral characteristic of the entire blast furnace. After a period of app. 10 mins, the production rate approaches a quasi-steady state with fluctuations of app. 0.1 kg/s. These fluctuations are caused by the highly unsteady flow and transfer conditions in the furnace and the discontinuity of the melting process which is shown in the following Fig. 6 - 8 for a representative ore particle in the vicinity of the cohesive zone. These figures highlight the depth of resolution of the XDEM simulation platform because the thermodynamic state of each particle over its lifetime is determined based on first principles and monitored and are only available through the Euler-Lagrange approach. Mimicking this behaviour in a continuum model by additional closure relations is a tedious effort that most probably fails to represent the large variety of particle states.

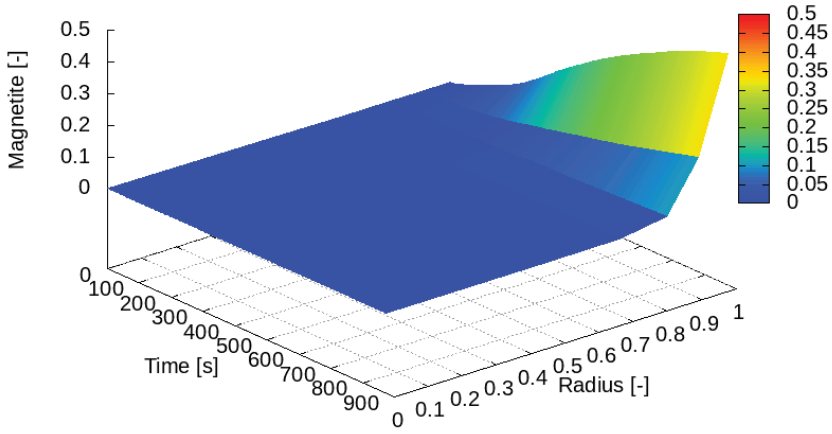

FIGURE 8. Magnetite profile versus time and radius in an ore particle near the cohesive zone

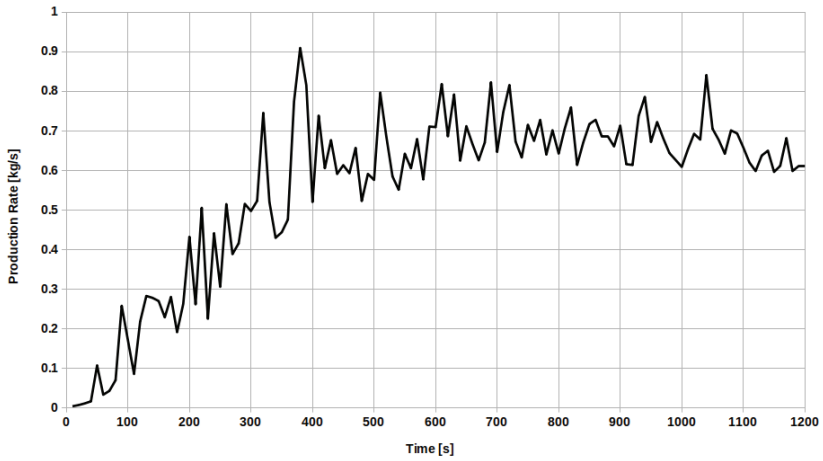

FIGURE 9. Evolution of the production rate e.g. melting rate of the blast furnace starting from initial conditions similar to blowing-in

The following Fig. 10 depicts the evolution of coke, haematite and iron. While the mass of hematite and coke decrease due to reduction and oxidation, respectively, the solid mass of iron increases despite the melting in the cohesive zone. Thus, the melting rate is the limiting factor for the production rate which is at least difficult or even impossible to identify through measurements.

The limiting factor of the melting rate is also confirmed by the spatial temperature distribution of both gas phase and particle surface temperature depicted in a vertical slice through the centre of the furnace in Fig. 11.

Both, particle surface and gas temperature experience a rather sharp gradient over the region of the cohesive zone. The particle surface temperature drops from app. 2400 K to app. 1400 K, while the gas temperature decreases from app. 2000 K to app. 1400 K which is close to the melting temperature. This rapid change in temperature indicates that a maximum of heat is transferred to the particle and, thus, limits the melting i.e. production rate of the furnace.

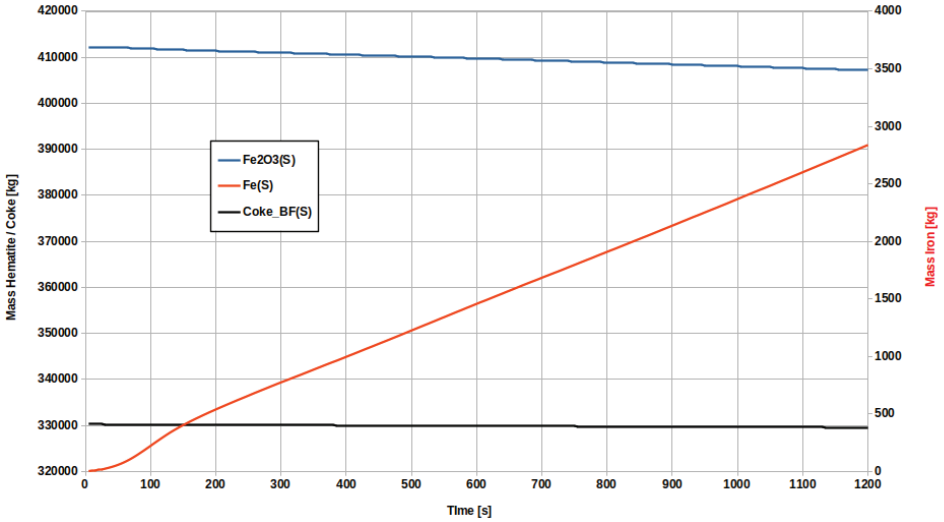

FIGURE 10. Evolution of the integral mass of haematite, solid iron and coke in the blast furnace

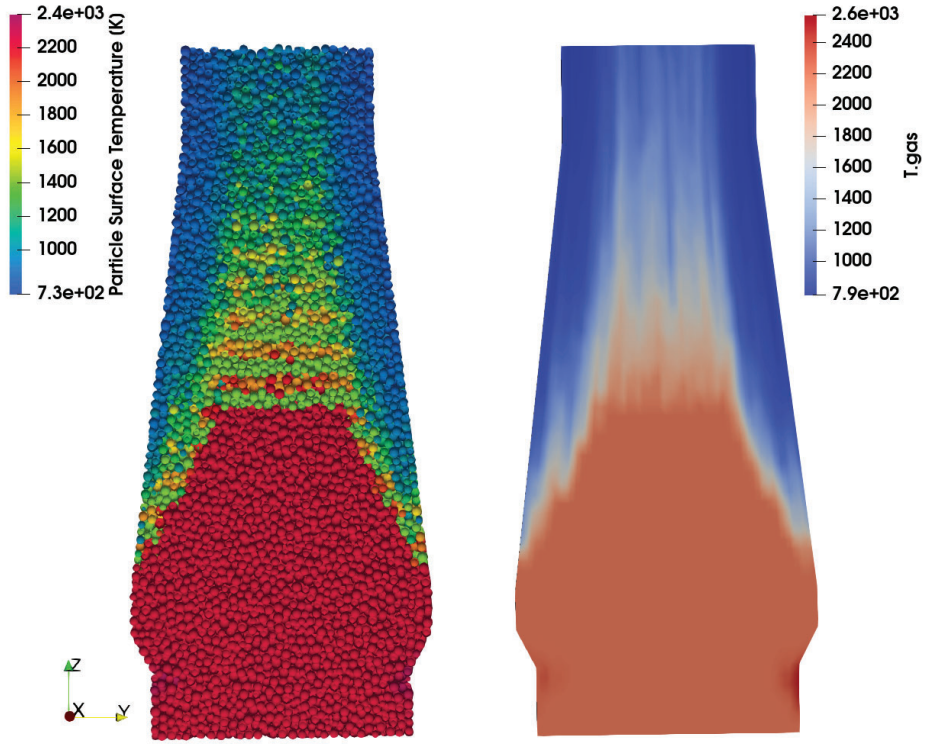

FIGURE 11. Distribution of particle surface temperature (left) and gas temperature in a vertical slice through the centre of the blast furnace.

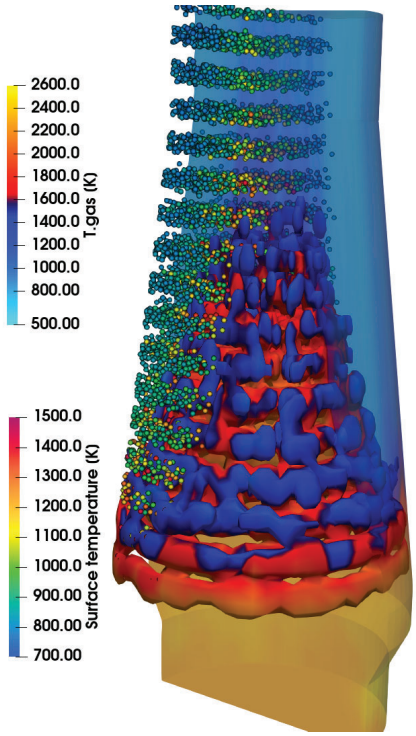

FIGURE 12. Shape and location of the cohesive zone represented by an iso-surface of the mass transfer rate of molten iron from the iron bearing particles to the liquid phase of the Euler solver in a vertical slice through the centre of the blast furnace. In addition, the gas temperature and ore particle layers with its surface temperature are depicted in a reduced particle size for better visibility.

Consequently, a higher production rate is achieved by increased heat transferred to the particles for which options are a higher blast flow rate or oxygen enrichment. This rapid temperature change is also visible in the cohesive zone shown in Fig. 12.

It shows the iron bearing particle layers at a reduced size for better visibility. These particles experience after the reduction process a further heat transfer that eventually leads to the formation of liquid iron in a particle. Available liquid material is transferred into the respective liquid phase of the multi-phase Euler solver and appears there as a mass source. It is shown in Fig. 12 as an iso-surface on which the gas temperature shown in Fig. 11 is projected. Hence, the location and shape of the cohesive zone is unambiguously defined by the production rate of liquid material at respective particle positions. The currently applied Euler method obviously is not able to resolve free surfaces of the liquid material as it trickles down the blast furnace. However, it is believed that tracking the liquid materials by volume fractions is sufficiently accurate, in particular that largely unknown material properties such as viscosity, surface tension and contact angle between liquid and solid surface versus temperature of liquids aggravate an accurate prediction of liquid surfaces.

The gas temperature projected onto the iso-surface highlights the large temperature difference of app. 1200 K in the region of the cohesive zone. This phenomenon emphasizes also the fact that a specific temperature or even small temperature range in entirely continuum based approaches is hardly suited to locate the cohesive zone. A resolution of the cohesive zone with its variation in temperatures, final reduction of iron oxides and discontinuous melting due at a melting temperature is only achieved by the currently applied Euler-Lagrange approach that is based on first principles without any further assumption for the development of the cohesive zone.

Closely connected to the reduction of iron bearing material according to eqs 4 to 6 is the distribution of carbon monoxide and dioxide depicted in a vertical slice though the centre of the blast furnace in Fig. 13 and Fig. 14.

Both figures show a layered structure for the carbon monoxide and dioxide distributions that is caused by the reduction in the ore layers and the Boudouard reaction in the coke layers. Carbon monoxide is transferred from the gas phase to the ore particles and, thus leading to a reduction of iron ores. It results in a formation of carbon dioxide that then is released to the gas phase by a transfer from the particle surface to the surrounding gas. The carbon dioxide

is transported into the next upper coke layer where the Boudouard reaction takes place dependent on the temperature of the coke layer to decrease the carbon dioxide and increase the carbon monoxide concentration. Newly generated carbon monoxide streams into the next ore layer where it is available for further reduction reactions. This mechanism repeats itself in the shaft of the furnace, however, with decreasing efficiency due to falling temperatures.

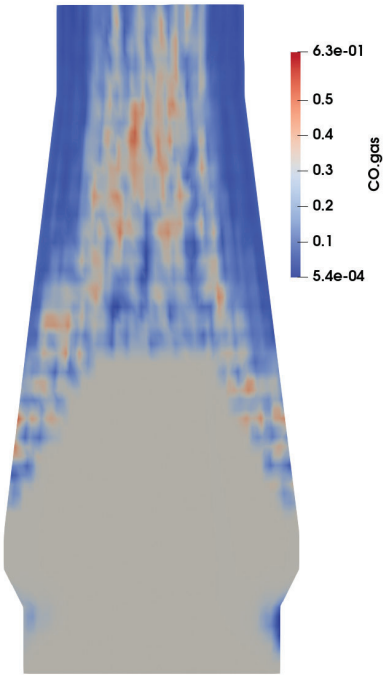

FIGURE 13. Distribution of carbon monoxide in a vertical slice through the centre of the blast furnace.

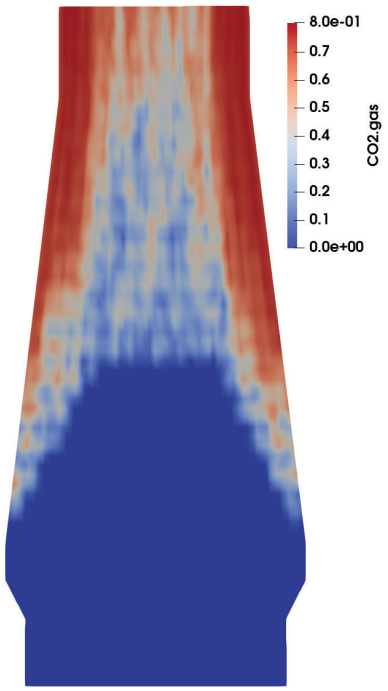

FIGURE 14. Distribution of carbon dioxide in a vertical slice through the centre of the blast furnace.

SUMMARY

The applied XDEM simulation environment couples the "best-of-the-class" single-physics software modules for multi-physics applications. In the current application, a DEM module for predicting the motion of particles, the XDEM module evaluating the thermal state of coke and iron-bearing particles and OpenFoam as the CFD module to predict the fluid and thermodynamic state of the multi-phase flow in the void space of the blast furnace were connected via an interface. The latter controls heat, mass and momentum transfer between the individual modules. Combining this concept with fast algorithms for evaluation in each module in conjunction with innovative partitioning technologies enables digital twins for production blast furnaces. Hence, the concept of smart virtual prototyping (SVP) by multi-physics simulations already support design and operation conditions at a very early sate during the initial design phase, not only limited to blast furnaces but also applicable to thermal treatment of particulate material such as biomass furnaces or additive manufacturing. These studies may be extended through the lifetime of a blast furnace accommodating changes in design and operating conditions. Results obtained from digital twins allow decision makers to take informed decisions leading to a competitive edge in the market.

ACKNOWLEDGMENTS

The authors would like to extend his gratitude to all members, past and current of the XDEM team who contributed to the Extended Discrete Element Method (XDEM). Furthermore, the research programs of the European Community, Fonts National de la Recherche of Luxembourg and the High Performance Computer centre of the University of

Luxembourg is greatly acknowledged for their continuous support.

REFERENCES

1. "Top 10 strategic technology trends for 2017," https://www.gartner.com/newsroom/id/3482617, accessed: 2018-02.
2. Adhav, P., Besseron, X., and Peters, B., "Investigation of cfd-dem-fem momentum coupling results for awjc nozzle using precice," in *Multiphysics Conference 2023* (2023).
3. Aho, M., "Pyrolysis and combustion of wood and peat as a single particle and a layer," VTT Report **465** (1987).
4. Aminnia, N., Adhav, P., Darlik, F., Mashhood, M., Saraei, S. H., Besseron, X., and Peters, B., "Three-dimensional cfd-dem simulation of raceway transport phenomena in a blast furnace," Fuel **334**, 126574 (2023).
5. Arroyo, J., Perez, L., and Cuervo-Pinera, V., "Cfd modeling and validation of blast furnace gas/natural gas mixture combustion in an experimental industrial furnace," Processes **11**, 332 (2023).
6. author,, "title," **volume**, 688–696.
7. Babich, A., Senk, D., Guldenau, H. W., and Mavrommatis, K. T., *Ironmaking*.
8. Baniasadi, M., Baniasadi, M., and Peters, B., "Coupled CFD-DEM with Heat and Mass transfer to Investigate the Melting of a Granular Packed Bed," Chemical Engineering Science (2017), 10.1016/j.ces.2017.12.044.
9. Baniasadi, M. and Peters, B., "Preliminary investigation on the capability of extended discrete element method for treating the dripping zone of a blast furnace," ISIJ International **58** (2017).
10. Baniasadi, M. and Peters, B., "Resolving multiphase flow through packed bed of solid particles using extended discrete element method with porosity calculation," Industrial and Engineering Chemistry (2017), 10.1021/acs.iecr.7b02903.
11. Baniasadi, M., Peters, B., Baniasadi, M., and Besseron, X., "Hydrodynamic analysis of gas-liquid-liquid-solid reactors using the xdem numerical approach," Canadian Journal of Chemical Engineering (2018), 10.1002/cjce.23191.
12. Baniasadi, M., Peters, B., Pierret, J.-C., Vanderheyden, B., and Ansseau, O., "Experimental and numerical investigation into the softening behavior of a packed bed of iron ore pellets," Powder Technology **339**, 863–871 (2018).
13. Blevins, R. D., *Applied Fluid Dynamics Handbook* (Krieger Publishing Company, Malabar, Florida, 1984) pp. 493–509.
14. Brulin, J., Gasser, A., Rekik, A., Blond, E., and Roulet, F., "Thermomechanical modelling of a blast furnace hearth," Construction & building materials **326**, 126833– (2022).
15. Chu, Y. and Gao, C., "Data-based multiscale modeling for blast furnace system," AIChE journal **60**, 2197–2210 (2014).
16. Cundall, P. A. and Strack, O. D. L., "A discrete numerical model for granular assemblies," Geotechnique **29**, pp. 47–65 (1979).
17. Dong, X. F., Jayasekara, A., Sert, D., Ferreira, R., Gardin, P., Monaghan, B. J., Chew, S. J., Pinson, D., and Zulli, P., "Investigation of molten liquids flow in the blast furnace lower zone: Numerical modelling of molten slag through channels in a packed bed," Metallurgical and materials transactions. B, Process metallurgy and materials processing science **52**, 255–266 (2021).
18. Dullien, F. A. L., *Porous Media Fluid Transport and Pore Structure* (Academic Press, San Diego, 1979).
19. Estupinan Donoso, A. A., Hoffmann, F., and Peters, B., "Extended discrete element method used for convective heat transfer predictions," International Review of Mechanical Engineering **7**, 329–336 (2013).
20. Feng, Y.-H., Zhang, Z., Qiu, L., and Zhang, X.-X., "Heat recovery process modelling of semi-molten blast furnace slag in a moving bed using xdem," Energy (Oxford) **186**, 115876– (2019).
21. Ferzinger, J. H. and Peric, M., *Computation Methods for Fluid Dynamics* (Springer Verlag, Heidelberg, 1996).
22. Fu, D., Chen, Y., Zhao, Y., D'Alessio, J., Ferron, K. J., and Zhou, C. Q., "Cfd modeling of multiphase reacting flow in blast furnace shaft with layered burden," Applied thermal engineering **66**, 298–308 (2014).
23. Fu, D., Tang, G., Zhao, Y., D'Alessio, J., and Zhou, C. Q., "Modeling of iron ore reactions in blast furnace," International journal of heat and mass transfer **103**, 77–86 (2016).
24. Gidaspow, D., *Multiphase flow and Fluidisation* (Academic Press, 1994).
25. Grejtak, T., Wang, S., and Shao, J., "Modeling of a blast furnace with both cfd and thermodynamics principles," Applied Mechanics **3**, 1019–1039 (2022).
26. Grønli, M., *A theoretical and experimental study of the thermal degradation of biomass*, Ph.D. thesis, NTNU Trondheim (1996).
27. Hoffmann, F., *Modelling Heterogeneous Reactions In Packed Beds And Its Application To The Upper Shaft Of A Blast Furnace*, Phd (2014).
28. Hou, Q., Dianyu, E., Kuang, S., Li, Z., and Yu, A., "Dem-based virtual experimental blast furnace: A quasi-steady state model," Powder Technology (2016).
29. Jiao, L., Kuang, S., Liu, L., Yu, A., Li, Y., Mao, X., and Xu, H., "Cfd modeling and analysis of particle size reduction and its effect on blast furnace ironmaking," Metallurgical and materials transactions. B, Process metallurgy and materials processing science **52**, 138–155 (2021).
30. Jiao, L., Kuang, S., Yu, A., Li, Y., Mao, X., and Xu, H., "Three-dimensional modeling of an ironmaking blast furnace with a layered cohesive zone," Metallurgical and materials transactions. B, Process metallurgy and materials processing science **51**, 258–275 (2020).
31. Jimbo, I. and Cramb, A. W., "The density of liquid iron-carbon alloys," Metallurgical Transactions B **24**, 5–10 (1993).
32. Krause, B., Liedmann, B., Wiese, J., Bucher, P., Wirtz, S., Piringer, H., and Scherer, V., "3D-DEM-CFD simulation of heat and mass transfer, gas combustion and calcination in an intermittent operating lime shaft kiln," International Journal of Thermal Sciences (2017), https://doi.org/10.1016/j.ijthermalsci.2017.03.017.
33. Kuang, S., Li, Z., and Yu, A., "Review on modeling and simulation of blast furnace," Steel research international **89**, 1700071–n/a (2018).
34. Li, J., Hua, C., Yang, Y., and Guan, X., "A novel mimo t-s fuzzy modeling for prediction of blast furnace molten iron quality with missing outputs," IEEE transactions on fuzzy systems **29**, 1654–1666 (2021).
35. Li, J., Kuang, S., Jiao, L., Liu, L., Zou, R., and Yu, A., "Numerical modeling and analysis of hydrogen blast furnace ironmaking process," Fuel (Guildford) **323**, 124368– (2022).
36. Li, J., Zhu, R., Zhou, P., Song, Y.-p., and Zhou, C. Q., "Prediction of the cohesive zone in a blast furnace by integrating cfd and svm modelling," Ironmaking & steelmaking **48**, 284–291 (2021).

37. Mahmoudi, A. H., Besseron, X., Hoffmann, F., Markovic, M., and Peters, B., "Modeling of the biomass combustion on a forward acting grate using xdem," Chemical Engineering Science **142**, 32–41 (2016).
38. Mahmoudi, A. H., Hoffmann, F., Markovic, M., Peters, B., and Brem, G., "Numerical modeling of self-heating and self-ignition in a packed-bed of biomass using xdem," Combustion and Flame **163**, 358–369 (2016).
39. Mahmoudi, A. H., Hoffmann, F., and Peters, B., "Semi-resolved modeling of heat-up, drying and pyrolysis of biomass solid particles as a new feature in xdem," Applied Thermal Engineering **93**, 1091–1104 (2016).
40. Mohanty, T., Sahoo, S., and Moharana, M., "Computational modeling of blast furnace stave cooler based on steady state heat transfer analysis," Procedia Engineering **127**, 940–946 (2015).
41. Mohseni, M., Kolomijtschuk, A., Peters, B., and Demoulling, M., "Biomass drying in a vibrating fluidized bed dryer with a lagrangian-eulerian approach," International Journal of Thermal Sciences **138**, 219 – 234 (2019).
42. Moysey, P. A. and Thompson, M. R., "Modelling the solids inflow and solids modification conveying of single-screw extruders using the discrete element method," Powder Technology **151**, 44 (2005).
43. N., W. and S., K., *Heat and Mass Transfer in Packed Beds* (Gordon and Breach, Philadelphia, 1982).
44. Okosun, T., Silaen, A. K., and Zhou, C. Q., "Review on computational modeling and visualization of the ironmaking blast furnace at purdue university northwest," Steel research international **90**, 1900046–n/a (2019).
45. Monteiro de Oliveira, M. J., Rodrigues, G. F. R., Silva, I. A., Peixoto, J. J. M., and Silva, C. A. d., "Modeling of two-phase flow in blast furnace trough," Steel research international **92**, 2000485–n/a (2021).
46. Patankar, S. V., *Numerical Heat Transfer and Fluid Flow* (McGraw-Hill Book Company, New York, 1980).
47. Peters, B., "Numerical simulation of heterogeneous particle combustion accounting for morphological changes," in *27th International Conference on Environmental Systems, Lake Tahoe, USA, SAE-paper 972562* (1997).
48. Peters, B., "Classification of combustion regimes in a packed bed based on the relevant time and length scales," Combustion and Flame **116**, 297 – 301 (1999).
49. Peters, B., "Classification of combustion regimes in a packed bed of particles based on the relevant time and length scales," Combustion and Flame **116**, 297–301 (1999).
50. Peters, B., "Measurements and application of a discrete particle model (dpm) to simulate combustion of a packed bed of individual fuel particles." Combustion and Flame **131**, 132–146 (2002).
51. Peters, B., *Thermal Conversion of Solid Fuels* (WIT Press, 2003).
52. Peters, B., *Thermal Conversion of Solid Fuels* (WIT Press, Southampton, 2003).
53. Peters, B., "The extended discrete element method (xdem) for multi-physics applications," Scholarly Journal of Engineering Research **2**, 1–20 (2013).
54. Peters, B., "The first unified and transient modelling platform to build a digital twin of blast furnaces based on the extended discrete element method (xdem)," Steel Research International (2023).
55. Peters, B., Baniasadi, M., Baniasadi, M., Besseron, X., Donoso, A. E., Mohseni, M., and Pozzetti, G., "XDEM multi-physics and multi-scale simulation technology: Review of DEM-CFD coupling, methodology and engineering applications," Particuology (2018), https://doi.org/10.1016/j.partic.2018.04.005.
56. Peters, B., Besseron, X., A. Estupinan Donoso, A. A., Hoffmann, F., Michael, M., and Mahmoudi, A. H., "Enhanced thermal process engineering by the extended discrete element method (xdem)," Universal Journal of Engineering Science **1**, 139–145 (2013).
57. Peters, B., Besseron, X., Estupinan Donoso, A. A., Mahmoudi, A. H., and Mohseni, S., "A discrete/continuous numerical approach to multi-physics," IFAC-PapersOnLine **28**, 645–650 (2015).
58. Peters, B. and Bruch, C., "A flexible and stable numerical method for the decomposition process of wood particles." Chemosphere **42**, 481–490 (2001).
59. Peters, B. and Donoso, A. E., *Why Do - Discrete Element Analysis?* (NAFMS, ISBN 978-1-910643-43-3, 2018).
60. Peters, B. and Dziugys, A., "Numerical simulation of the motion and combustion of granular material." Industrial Heat Engineering **21**, 109–113 (1999).
61. Peters, B. and Hoffmann, F., "Iron ore reduction predicted by a discrete approach," Chemical Engineering Journal **304**, 692–702 (2016).
62. Peters, B., Hoffmann, F., Senk, D., Babich, A., Hausemer, L., and Simoes, J.-P., "A combined experimental and numerical approach to a discrete description of indirect reduction of iron oxide," LA METALLURGIA ITALIANA , 49–54 (2016).
63. Peters, B., Hoffmann, F., Senk, D., Babich, A., Simoes, J., and Hausemer, L., "Experimental and numerical investigation into iron ore reduction in packed beds," Chemical Engineering Science (2015).
64. Peters, B. and Pozzetti, G., "Flow characteristics of metallic powder grains for additive manufacturing," EPJ Web of Conferences **13001**, 140 (2017).
65. Phuc, P. V., Chiba, S., and Minami, K., "Large scale transient cfd simulations for buildings using openfoam on a world's top-class supercomputer," in *4th OpenFOAM User Conference 2016* (2016).
66. Pozzetti, G., Besseron, X., Rousset, A., and Peters, B., "A co-located partitions strategy for parallel cfd–dem couplings," Advanced Powder Technology **29**, 3220–3232 (2018).
67. Pozzetti, G., Besseron, X., Rousset, A., and Peters, B., "A parallel multiscale dem-vof method for large-scale simulations of three-phase flows," Proceedings of ECCM-ECFD 2018 (2018).
68. Pozzetti, G., Jasak, H., Besseron, X., Rousset, A., and Peters, B., "A parallel dual-grid multiscale approach to cfd–dem couplings," Journal of Computational Physics **378**, 708–722 (2019).
69. Pozzetti, G. and Peters, B., "Evaluating erosion patterns in an abrasive water jet cutting nozzle using xdem," Advances in Powder Metallurgy & Particulate Materials , 191–205 (2017).
70. Radjuk, A., Titlianov, A., and Skripalenko, M., "Computer simulation of temperature field of blast furnace's air tuyere," Computer Research and Modeling **9**, 117–125 (2017).
71. Roeplal, R., Pang, Y., Adema, A., van der Stel, J., and Schott, D., "Modelling of phenomena affecting blast furnace burden permeability using the discrete element method (dem) – a review," Powder technology **415**, 118161– (2023).
72. Saastamoinen, J., Aho, M., and Linna, V., "Simultaneous pyrolysis and char combustion," Fuel **72**, 599–609 (1993).

73. Saastamoinen, J., Huttunen,, and J.-R., R., "Simultaneous drying and pyrolysis of solid fuel particles," Combustion and Flame **106**, 288 – 300 (1998).
74. Saastamoinen, J. and Richard, J.-R., "Simultaneous drying and pyrolysis of solid fuel particles," Combustion and Flame **106**, 288–300 (1998).
75. Samiei, K. and Peters, B., "Experimental and numerical investigation into the residence time distribution of granular particles on forward and reverse acting grate," Chemical Engineering Science , 234–245 (2013).
76. Santana, E. R., Pozzetti, G., and Peters, B., "Application of a dual-grid multiscale cfd-dem coupling method to model the raceway dynamics in packed bed reactors," Chemical Engineering Science (2019).
77. Santata, E., Peters, B., and Pozzetti, G., "Application of a dual-grid multiscale cfd-dem coupling method to model the raceway dynamics in packed bed reactors," Chemical Engineering Science (2019).
78. Saruwatari, M. and Nakamura, H., "Coarse-grained discrete element method of particle behavior and heat transfer in a rotary kiln," Chemical Engineering Journal **428**, 130969 (2022).
79. Seebauer, V., *Experimentelle Untersuchungen zur Pyrolyse von Kohle und Holz*, Ph.D. thesis, Graz University of Technology (1999).
80. Shen, Y., Guo, B., Chew, S., Austin, P., and Yu, A., "Three-dimensional modeling of flow and thermochemical behavior in a blast furnace," Metallurgical and materials transactions. B, Process metallurgy and materials processing science **46**, 432–448 (2015).
81. Shih-I, P., *Two-Phase Flows* (Vieweg Tracts in Pure and Applied Physics, Braunschweig, 1977).
82. Tang, H., Meng, F., Zhao, Z., and Zhang, L., "Modeling coal/coke combustion behavior in tuyere-raceway-dripping zone in blast furnace," Procedia Engineering **102**, 1583–1592 (2015).
83. Vargas, W. L. and McCarthy, J. J., "Heat conduction in granular materials," AIChE Journal **47**, 1052 (2001).
84. Wang, S. and Shen, Y., "Cfd-dem modelling of raceway dynamics and coke combustion in an ironmaking blast furnace," Fuel (Guildford) **302**, 121167– (2021).
85. Watakabe, S., Miyagawa, K., Matsuzaki, S., Inada, T., Tomita, Y., Saito, K., Osame, M., Sikström, P., Ökvist, L. S., and Wikstrom, J.-O., "Operation trial of hydrogenous gas injection of course50 project at an experimental blast furnace," ISIJ International **53**, 2065–2071 (2013).
86. Watakabe, S., Miyagawa, K., Matsuzaki, S., Inada, T., Tomita, Y., Saito, K., Osame, M., Sikström, P., Ökvist, L. S., and Wikstrom, J.-O., "Operation trial of hydrogenous gas injection of course50 project at an experimental blast furnace," ISIJ International **53**, 2065–2071 (2013).
87. Weltry, j., Wicks, C. E., Rorrer, G. L., and WIlson, R. E., *Fundamentals of Momentgum, Heat and Mass Transfer*, 5th ed. (Wiley).
88. Yu, X. and Shen, Y., "Modelling of blast furnace with respective chemical reactions in coke and ore burden layers," Metallurgical and materials transactions. B, Process metallurgy and materials processing science **49**, 2370–2388 (2018).
89. Yu, X. and Shen, Y., "Transient state modeling of industry-scale ironmaking blast furnaces," Chemical engineering science **248**, 117185– (2022).
90. YUAN, M., ZHOU, P., LI, M.-l., LI, R.-f., WANG, H., and CHAI, T.-y., "Intelligent multivariable modeling of blast furnace molten iron quality based on dynamic aga-ann and pca," Journal of iron and steel research, international **22**, 487–495 (2015).
91. Zervas, T., McMullan, J. T., and Williams, B. C., "Solid-based processes for the direct reduction of iron," International Journal of Energy Research **20**, 255–278 (1996).
92. Zhou, C., Tang, G., Wang, J., Fu, D., Okosun, T., Silaen, A., and Wu, B., "Comprehensive numerical modeling of the blast furnace ironmaking process," JOM (1989) **68**, 1353–1362 (2016).
93. Zuo, H.-b., Wang, C., Dong, J.-j., Jiao, K.-x., and Xu, R.-s., "Reduction kinetics of iron oxide pellets with h2 and co mixtures," **22**, 688–696.